PCCP

Accepted Manuscript

Volume 18 | Number 1 | 7 January 2016 | Pages 1–636

PCCP

Physical Chemistry Chemical Physics
www.rsc.org/pccp

ISSN 1463-9076

PERSPECTIVE
Darya Radziuk and Helmuth Möhwald
Ultrasonically treated liquid interfaces for progress in cleaning and separation processes

175 YEARS

ROYAL SOCIETY OF CHEMISTRY

rsc.li/pccp

Complexation of halide ions to tyrosine: role of non-covalent interactions evidenced by IRMPD spectroscopy

Davide Corinti,[a] Barbara Gregori,[a] Leonardo Guidoni,[b] Debora Scuderi,[c] Terry McMahon,[d] Barbara Chiavarino,[a] Simonetta Fornarini,[a] Maria Elisa Crestoni[a],*

[a]Dipartimento di Chimica e Tecnologie del Farmaco, Università di Roma "La Sapienza", P.le A. Moro 5, I-00185 Roma, Italy
[b] Dipartimento di Scienza Fisiche e Chimiche, Università degli Studi dell'Aquila, Via Vetoio 2, Coppito, L'Aquila I-64100, Italy
[c]Laboratoire de Chimie Physique, Faculté des Sciences d'Orsay, Université Paris Sud, UMR8000, CNRS, Bat. 201 P2, 91405 Orsay Cedex, France.
[d]Department of Chemistry, University of Waterloo, 200 University Avenue West, Waterloo, Ontario, N2L 3G1

Abstract

The binding motifs in the halide adducts with tyrosine ([Tyr+X]$^-$, X = Cl, Br, I) have been investigated and compared with the analogues with 3-nitrotyrosine (nitroTyr), a biomarker of protein nitration, in a solvent-free environment by mass-selected infrared multiple photon dissociation (IRMPD) spectroscopy over two IR frequency ranges, namely 950-1950 and 2800-3700 cm^{-1}. Extensive quantum chemical calculations at B3LYP, B3LYP–D3 and MP2 levels of theory have been performed using the 6-311++G(d,p) basis set to determine the geometry, relative energy and vibrational properties of likely isomers and interpret the measured spectra. A diagnostic carbonyl stretching band at ~1720 cm^{-1} from the intact carboxylic group characterizes the IRMPD spectra of both [Tyr+X]$^-$ and [nitroTyr+X]$^-$, revealing that the canonical isomers (maintaining intact amino and carboxylic functions) are the prevalent structures.

The spectroscopic evidence reveals the presence of multiple non-covalent forms. The halide complexes of tyrosine conform to a mixture of plane and phenol isomers. The contribution of phenol-bound isomers is sensitive to anion size, increasing from chloride to iodide, consistent with the decreasing basicity of the halide, with relative amounts depending on the relative energies of the respective structures. The stability of the most favorable phenol isomer with respect to the reference plane geometry is in fact 1.3, -2.1, -6.8 kJ mol^{-1}, for X = Cl, Br, I, respectively. The change in π-acidity by ring nitration also stabilizes anion-π interactions yielding ring isomers for [nitroTyr+X]$^-$, where the anion is placed above the face of the aromatic ring.

1

Introduction

The importance of anion-amino acid interactions is well documented in biology playing a role in relevant functions such as neuron signaling, ion transport, drug-receptor recognition.[1,2] Although many proteins are commonly negatively charged, anionic amino acid clusters are much less studied than metal cation adducts. However, anion complexation also relies on hydrogen bonding, ion-dipole interactions, and hydrophobic effects which in principle may also preferentially stabilize zwitterionic forms relative to their neutral, canonical counterparts.[3] In addition, other non-covalent contacts, including anion-π effects favored between π-acidic arenes and charge-diffuse anions, may contribute in stabilizing negatively charged adducts of (aromatic) amino acids.

Recently, Infrared Multiple Photon Dissociation (IRMPD) spectroscopy,[4-7] a powerful tool to identify the structural and electronic features of various ionic species in the gas phase,[8-14] including mono-[15-16] and divalent-[17] metal-bound amino acids, has revealed canonical structures for halide adducts of glutamic acid, histidine, and phenylalanine.[18] In contrast arginine is rather in the zwitterionic form[19], and canonical and zwitterionic isomers are both significantly populated in the proline-chloride complex.[20] Different binding motifs have been also highlighted by IRMPD assay of halide adducts of 1,3,5-trinitrobenzene, a representative π–acidic arene, showing that: i) the fluoride adduct $[TNB + F]^-$ conforms to a strongly covalent σ-complex (Meisenhemer complex); ii) the chloride complex $[TNB + Cl]^-$ places the anion on the periphery of the aromatic ring;[21] the bromide $[TNB + Br]^-$ and iodide $[TNB + I]^-$ adducts display weakly covalent structures.[22,23]

The present study is focused on the bonding motifs of halide ions (Cl^-, Br^-, and I^-) with L-tyrosine (Tyr) and 3-nitro-tyrosine (nitroTyr), where phenolic ring nitration is a post-translational modification effected by reactive nitrogen species. The structure of deprotonated tyrosine, $[Tyr-H]^-$, interrogated by IRMPD spectroscopy has shown clear evidence of a carboxylate structure. This result is consistent with the fact that the phenoxide anion isomer is higher in energy by ca. 10 kJ mol^{-1} in the gas phase.[24] However, the gas phase structure of $[Tyr-H]^-$ is reported to depend on the (a)protic nature of the solvent used in the electrospray ionization.[25-27]

In addition, the protonated forms of tyrosine and of 3-NO_2-tyrosine have been assayed by IRMPD spectroscopy in two complementary IR frequency ranges showing unambiguous evidence of amino group protonation and characteristic absorptions associated to nitration.[28]

Herein, $[Tyr + X]^-$ and $[nitroTyr + X]^-$ (X = Cl, Br, I) complexes have been investigated to broaden the little-existing documentation about anion/amino acid interactions. The intrinsic properties of $[Tyr + X]^-$ ions have been inspected by IRMPD spectroscopy in the 950-1950 cm^{-1} range, exploiting the bright and tunable radiation from the free electron laser beamline at the CLIO (Centre Laser Infrarouge d'Orsay) facility, along with quantum chemical calculations to aid in the interpretation of the observed spectra. Additional spectroscopic information has been obtained in the 2800-3700 cm^{-1} range that is especially revealing of non-covalent interactions involving NH/OH bonds. Diagnostic vibrational features of tyrosine nitration are expected to be useful to reveal direct structural clues related to biological activity, including whether the (modified) amino acid adopts either a canonical, charge solvated or a zwitterionic, form in these complexes, whether anion-π interactions may contribute to stabilize the gas-phase population, and to what extent the ground state geometries are sensitive to the halide anion identity.

Methods

IRMPD spectroscopy

IRMPD spectra of halide adducts of (3-NO_2-)tyrosine were acquired employing two different experimental setups: i) a modified Paul ion-trap mass spectrometer (Bruker Esquire 3000+) equipped with an electrospray ionization ESI source and coupled to the IR radiation of a tunable (5-

2

25 μm) free electron laser (FEL) at CLIO[29]; ii) a tabletop KTP/KTA optical parametric oscillator/amplifier system (OPO/OPA, Laser Vision) whose radiation output is admitted into a modified Paul ion-trap mass spectrometer (Esquire 6000+, Bruker Daltonics), assembled at the Università di Roma "La Sapienza". Details on these integrated setups have been previously described.[30-32]

Solutions were prepared 30 μM NH_4X (X= Cl, Br, I) and 20 μM of either Tyr or nitroTyr in water: methanol (1:1), with 2% ammonia to assist deprotonation. All reagents were commercial products (Sigma-Aldrich srl Milan, Italy), used as received. A dilute solution 5 μM in each analyte was continuously infused into the ESI source at a flow rate of 2.5 μL min^{-1} to generate the halide clusters. In either ion trap, precursor ions were accumulated for 5-10 ms and mass-selected by resonance ejection prior to IR irradiation for: i) 0.2-0.5 s by the CLIO-FEL over the mid-IR range (950-1950 cm^{-1}); ii) 2 s by the OPO/OPA laser covering the NH/OH stretching region (2800-3700 cm^{-1}). The irradiation time is controlled by an electromechanical shutter synchronized with the mass spectrometer.

The FEL radiation is generated by a 10-50 MeV electron linear accelerator and delivered in 9 μs macropulses (25 Hz), each containing 600 micropulses (0.5–3 ps long). Typical macropulse energies are 40 mJ. For the present study, the electron energy was set to 44 MeV with a fairly stable laser power ranging from 1.1 to 0.8 W upon increasing frequency. The IR-FEL spectral width (fwhm) was less than 0.5% of the central wavelength.

The parametric converter is pumped using a Nd:YAG laser (Continuum Surelite II) running at 10 Hz and delivering 600 mJ per pulse (4–6 ns long). The typical output energy from the OPO/OPA laser was 18-20 mJ/pulse in the investigated spectral range with 3-4 cm^{-1} bandwidth.

A stepwise process based on the absorption of multiple resonant photons, associated with intramolecular vibrational energy redistribution, can heat the ions to a threshold energy for fragmentation, typically proceeding along the lowest energy pathway.[4]

By recording the abundances of the precursor ion (I_P) and of all fragment ions (I_F) as a function of the photon wavenumber, the IRMPD spectrum is collected as the photodissociation yield R, defined as $-\ln[I_P/(I_P + \Sigma I_F)]$.[33] Mass spectra were obtained by accumulation of five sequences and averaged over four at each photon energy, which was increased in steps of 4–5 cm^{-1}. In all the acquired spectra, a quantitative accord is verified between the reduction of the precursor ion signal and the increase of the product ion signals. A good overlap of the laser beam with the ion cloud has been observed.

Computational details

A preliminary conformational search to identify candidate low-energy isomers and conformers of [Tyr+X]$^-$ and [nitroTyr+X]$^-$ (X = Cl, Br, I) was carried out by performing 300 cycles of simulated annealing using tools of Amber8, Sander[34] with the GAFF (General Amber Force Field) force field.[35] For higher level optimization, low-energy geometries were sorted into families with similar non-covalent interactions, and those within 50 kJ mol^{-1} from the global minimum structure were fully optimized by means of density functional theory calculations at the B3LYP/6-311++G(d,p) level.

Harmonic vibrational frequency analysis was carried out on all optimized structures to characterize the stationary points as local minima, and to obtain linear IR spectra. In addition, zero-point energy (ZPE) and thermal corrections were also obtained at the same level of theory. In order to improve the agreement between experimental and calculated spectra, harmonic frequencies were uniformly scaled by using a factor of 0.978 (0.955) in the 950-1950 cm^{-1} (2800-3700 cm^{-1}) frequency region.[18] For the sake of comparison, calculated resonances were convoluted by assuming a Lorentzian profile with 20 cm^{-1} (5 cm^{-1}) full width at half-maximum (FWHM)) in the 950-1950 cm^{-1} (2800-3700 cm^{-1}) spectral range. Calculations on the complete set of conformers have been

also performed at B3LYP-D3/6-311++G(d,p) level as employed into the Spartan 16 suite of programs (Wavefunction, Inc., Irvine, CA). The Grimme dispersion correction was employed in order to account more accurately for non-covalent interactions, which may play a major role in the adducts subject of this work.

As the geometric and vibrational properties of the low-energy isomers and conformers of [Tyr+X]⁻ and [nitroTyr+X]⁻ do not present substantial changes using either B3LYP or B3LYP-D3, henceforth we will uniformly refer to the geometries and IR spectra obtained at the B3LYP/6-311++G(d,p) level.

In order to more accurately evaluate relative electronic energies, single-point energy calculations were also performed on the optimized B3LYP geometries at the MP2/6-311++G(d,p) level. We employed the ORCA 3.0.1 software package with a SCF convergence set as TightSCF (energy change 1e−08; max-density change 1e−07; rms-density change 5e−09; DIIS error 5e−07) and a high precision for the integration grids.[36-37]

An effective core potential (def2-TZVP) is employed in the MP2 calculations for the iodine atom.[38] MP2 refined relative enthalpies (or Gibbs free energies) were obtained by adding B3LYP thermal (298 K) and ZPE corrections to MP2 electronic energies and are denoted as MP2(full)//6-311++G(d,p)//B3LYP/6-311++G(d,p).

Results and discussion

Photodissociation mass spectra

Electrosprayed halide-bound complexes of L-tyrosine, and 3-NO₂-L-tyrosine have been mass-selected, trapped and studied by IRMPD spectroscopy, taking advantage of its potential to provide diagnostic clues that could integrate poorly informative collision induced dissociation (CID) assays. Upon absorption of resonant IR photons, the internal energy of the sampled species slowly increases, ultimately promoting a wavelength-dependent dissociation process along the lowest energy fragmentation route.[4, 39-40]

The photofragmentation of chloride adducts [Tyr+Cl]⁻ (*m/z* 216/218) and [nitroTyr+Cl]⁻ (*m/z* 261/263) in both the explored fingerprint and NH/OH stretching ranges involves the loss of HCl, which leads to deprotonated tyrosine, [Tyr-H]⁻ (*m/z* 180), and 3-NO₂-tyrosine, [nitroTyr-H]⁻ (*m/z* 225), as displayed in the mass spectra obtained when [Tyr+Cl]⁻ and [nitroTyr+Cl]⁻ are irradiated at the IR-active frequency of 1505 and 1477 cm⁻¹, respectively (Fig. S1(a) and S2(a)). However, the relatively low mass cut off of the ion trap mass spectrometer used precluded the possibility to reveal the product ion at m/z 35/37 [Cl]⁻. As a matter of fact, the evidence that the signal depletion detected in the parent ion channel, [Tyr+Cl]⁻, largely exceeds the ion abundance change in the fragment ion channel, [Tyr-H]⁻, is indicative that the photofragmentation also proceeds by the blind fragment channel [Cl]⁻ involving loss of neutral tyrosine (Fig. S3).

Despite this blind dissociation channel, the neat correspondence in the position of the features in both the parent ion depletion and the fragment ion profile confirms that the [Cl]⁻ dissociation path presents the same vibrational features as the [Tyr-H]⁻ fragmentation channel. This evidence has enabled us to present the IRMPD spectra of [Tyr+Cl]⁻ and [nitroTyr+Cl]⁻ by recording the photofragmentation yield R as a function of the photon energy (see below) relying on the abundance of the [Tyr-H]⁻ as only fragment.

In contrast, the assayed bromide, [Tyr+Br]⁻ (*m/z* 260/262) and [nitroTyr+Br]⁻ (*m/z* 305/307), and iodide, [Tyr+I]⁻ (*m/z* 308) and [nitroTyr+I]⁻ (*m/z* 353), complexes fragment by loss of intact amino acid and release of halide anions, Br⁻ and I⁻, as photofragments.

The exemplary mass spectra collected after exposure of tyrosine, [Tyr+Br]⁻ and [Tyr+I]⁻, and 3-nitrotyrosine, [nitroTyr+Br]⁻ and [nitroTyr+I]⁻, adducts to IR photons tuned at 1297 and 1177 cm⁻¹,

and to 1325 and 1737 cm^{-1} are presented in Fig. S1(b-c) and Fig. S2(b-c), respectively. The same fragmentation pattern is found when [Tyr+X]$^-$ and [nitroTyr+X]$^-$ (X = Cl, Br, I) are assayed by low-energy CID.

This behavior conforms to the lower binding energy with increasing anion size from Cl$^-$ to I$^-$, according to the calculated halide-ion dissociation energies reported in Table S1, combined with the stronger gas-phase acidity of HX ($\Delta G°_{acid}$) of HBr (1332 kJ/mol)[41] and HI (1294 kJ/mol)[42] as compared to HCl (1372 kJ/mol).[43] Notably, the same fragmentation channels have been recently observed upon IRMPD assay of halide-bound histidine, [His+X]$^-$ (X= Cl, Br, I),[19] and phenylalanine, [Phe+Cl]$^-$,[18] adducts.

IRMPD spectroscopy

A structural characterization of [Tyr+X]$^-$ (X = Cl, Br, I) complexes as naked species was sought by IRMPD spectroscopy performed in the fingerprint region (950−1950 cm^{-1}), a range which encompasses highly informative modes, including COH and NH bending vibrations along with carbonyl C=O and carboxylate OCO stretches.

As illustrated in Fig. 1, the IRMPD spectra of [Tyr+Cl]$^-$, [Tyr+Br]$^-$ and [Tyr+I]$^-$ exhibit similar profiles with several common features, including the pronounced bands around 1178, 1250, 1507, and 1608 cm^{-1}. However, some notable systematic shifting in the band positions and relative intensities appear with increasing anion size from Cl$^-$ to I$^-$, overall allowing a distinction of these complexes. In the low wavenumber region, the strong, poorly resolved absorbances centred at 1312 and 1376 cm$^-$ for [Tyr+Cl]$^-$ become even broader with increasing anion size (from ~90 to ~170 cm^{-1} fwhm), up to progressively encompass the weak band at ca. 1250 cm^{-1} in the case of [Tyr+I]$^-$. In the higher frequency side, the peak at 1720 cm^{-1} for [Tyr+Cl]$^-$ steadily shifts to 1730 for [Tyr+Br]$^-$ and 1750 cm^{-1} [Tyr+I]$^-$, whereas the small shoulder observed as a separate band at 1790 cm^{-1} for [Tyr+Cl]$^-$, progressively magnifies, appearing as a still distinct band at 1775 cm^{-1} for [Tyr+Br]$^-$, and as a strong, almost merged feature at 1785 cm^{-1} in the case of [Tyr+I]$^-$. These bands, definitely outside the range for antisymmetric carboxylate stretching mode, expected near 1635 cm^{-1} for deprotonated tyrosine,[26] rather correspond to the CO stretching mode of a carboxylic group, and closely approach v(CO) of chloride-bound phenylalanine (1710 cm^{-1}),[18] thus implying that also tyrosine is predominantly non-zwitterionic in these halide complexes. This motif is also supported by the lack in [Tyr+X]$^-$ of a signature for protonation at the amino group, namely the NH$_3^+$ umbrella mode observed at 1420 cm^{-1} in protonated tyrosine,[28] and by the position of the COH in-plane bending mode of the carboxylic group at ca. 1358-1375 cm^{-1}. The latter frequencies are in very good agreement with a related absorption observed at 1360 cm^{-1} for chloride-bound phenylalanine, previously interpreted as a diagnostic feature of halide-carboxylic hydrogen interaction.[18]

Interestingly, a charge solvated (CS) canonical structure with a tridentate N/O/ring structure as the preferred binding geometry for K$^+$-tagged tyrosine was also unveiled by IRMPD spectroscopy, with v(CO) at 1744 cm^{-1}.[44] The lower v(CO) frequency of [Tyr+Cl]$^-$ relative to the value found for [Tyr+K]$^+$ entails significantly different modes of interaction between the amino acid and the monoatomic ions, as already observed in analogous phenylalanine adducts.

Herein, the effect of a change in π-acidity on halide-tyrosine recognition has been also investigated by recording the IRMPD spectra of [nitroTyr+X]$^-$ (X= Cl, Br, I) adducts (Fig. 1).

The spectra exhibit common features, including the prominent, broad peak (~100 cm^{-1} fwhm) at 1316/1330 cm^{-1}, the intense, sharp absorption at 1528/1540 cm^{-1}, and the strong band at 1710 cm^{-1} for [nitroTyr+Cl]$^-$, which progressively shifts to 1733 cm^{-1} for [nitroTyr+Br]$^-$, and to 1743 cm^{-1} for [nitroTyr+I]$^-$. In addition, the weaker resonances of [nitroTyr+Cl]$^-$ observed at 1220, 1474, 1572, and 1610 cm^{-1} are almost the same for the three complexes, with frequency variations of less than 15 cm^{-1}, whereas an additional peak around 1700 cm^{-1} appears only in the case of [nitroTyr+X]$^-$

(X= Br⁻, I⁻). A few notable differences with the native [Tyr+X]⁻ adducts, likely associated to the nitration modification, are: i) the absence of any detectable features at 1180 cm⁻¹ and 1774-1790 cm⁻¹; ii) the presence of a broad intense band at 1316-1330 cm⁻¹ instead of the two partially resolved features at 1312 and 1375 cm⁻¹.

Spectroscopic information in the NH/OH range (2800−3700 cm⁻¹) has also been obtained for two examples of tyrosine adducts, [Tyr+X]⁻ (X = Cl, Br), as illustrated in Fig. S4 and S5, respectively, in the Supporting Information (SI). In this region, the two sampled adducts share very similar features, with a sharp (fwhm = 10 cm⁻¹), intense peak at 3663 cm⁻¹, a signature of the free OH of the phenol group, together with broad resonance structures at ca. 3200 and 3000 cm⁻¹, more conspicuous for X = Br.

For each sampled halide adduct, the IRMPD process can be very efficient in both the explored regions, leading to considerable signal depletion of the precursor ion population, whose trend neatly follows the appearance of the detected fragments.

Calculated structures

[Tyr+X]⁻ (X = Cl, Br, I)

An extensive conformational search aimed at collecting the low-energy structures for [Tyr+X]⁻ complexes has led to identify families of isomers arising from charge solvated (CS) or salt bridge (SB) structures, where X⁻ may interact with either the phenolic or carboxylic hydroxyl group, the amino hydrogens, the phenyl ring, or the ammonium ion. In addition to the different binding sites, one needs to consider two variants, differing in the orientation of the phenolic hydroxyl group which may lean either towards (*right*) or away from (*left*) the side of the amino group. However, as previously observed, the ensuing rotamers lie within 1 kJ mol⁻¹,[45-46] and henceforth we will preferentially refer to the usually lowest energy *left* variant.

The optimized geometries of the lowest energy canonical and zwitterion structures for [Tyr+Cl]⁻ obtained at the B3LYP/6-311++G(d,p) level of theory are shown in Fig. 2, along with their relative enthalpy (ΔH°_{rel}) and free energy (ΔG°_{rel}) values at 298 K calculated at the same level. In addition, further check at B3LYP-D3/6-311++G(d,p) level and single point energy calculations at MP2//B3LYP/6-311++G(d,p) have been carried out in order to account for dispersive interactions and to clarify the importance of the exact exchange energy in the interpretation of the system.[47-48] Fig. S6 and Table S2 provide comprehensive geometric and thermodynamic information on these and other conformational variants, deriving from systematic stepwise rotation of each torsional angle in the flexible skeleton of [Tyr+Cl]⁻. There is an overall reasonable agreement among all levels of theory in predicting as most favorable the canonical structures, with either a phenol, plane or terminal halide binding site. However, while the same trend in relative energy is envisioned by the two DFT levels of theory, MP2 data favor the bidentate plane relative to mono dentate phenol arrangements. This finding reflects the delicate energetic balance between these structures.[18, 49]

Although the averaged population at 298 K is very sensitive to the theoretical description, however the close energy spacing predicted at any level implies that more than a single structure would contribute to the thermal ion population at 298 K.

Henceforth, we will uniformly refer to Gibbs free energy values at 298 K at MP2 level, due to the comparatively improved accuracy in the treatment of non-covalent interactions.

In the lowest energy structure (**TCl_pla1**), the ∠O1C1C2N and ∠NC2C3C1' dihedral angles, equal to 157.1° and -67.3° (Table S3), respectively, allow a *gauche* conformation (meaning the relationship between NH₂ and the aromatic ring along the C2-C3 bond) with the phenol OH turned *left* with respect to the amino group, and the anion bound in a bidentate CH···Cl⁻···HOC(O) arrangement to both an aromatic hydrogen ($r_{Cl\cdots HC}$ = 2.68 Å) and the carboxylic OH group in *trans*

6

configuration ($r_{\text{Cl}\cdots\text{HOC(O)}}$ = 1.96 Å). The amino unit, flipping apart from the ring toward the carbonyl oxygen, is engaged in a hydrogen bond interaction ($r_{\text{CO}\cdots\text{HN}}$ = 2.31 Å).

The *gauche* monodentate species (**TCl_phe1**), located 1.3 kJ mol^{-1} above **TCl_pla1**, is endowed with a Cl$^{-}\cdots$HO motif, where chloride is bound to a *left* phenol OH ($r_{\text{Cl}\cdots\text{HOC}}$ =1.98 Å), and the carboxylic OH in a *trans* configuration is hydrogen bonded with the N terminus ($r_{\text{N}\cdots\text{OHC(O)}}$ = 1.86 Å). This arrangement brings the $\angle$O1C1C2N dihedral angle to 10.2°, leaving the $\angle$ NC2C3C1' almost unperturbed (-56.5°).

A decrease of the relative stability of only 1.1 kJ mol^{-1} is found by reversing the orientation of the phenol group so as to provide a *right* conformer (**TCl_phe2**). Notably, both these structures are stabilized by a weak N−H$\cdots\pi$ interaction due to the amino hydrogens pointing towards the aromatic ring. In the neutral amino acid, similar favourable O-H$\cdots$N and NH$\cdots\pi$ contacts were already predicted,[50-51] and identified in laser ablated jet cooled amino acid by microwave,[52] and electronic[53-55] spectroscopy.

The lowest energy terminal isomer (**TCl_ter1**), placed 7.0 kJ mol^{-1} higher in free energy than the global minimum, presents an *anti* NH$\cdots$Cl$^{-}\cdots$HOC(O) arrangement, which modifies both the $\angle$O1C1C2N and $\angle$NC2C3C1' dihedral angles to -57.6° and -176.7°, respectively, enabling chloride binding to the aminoacid terminal sites, i.e. the carboxylic acid ($r_{\text{Cl}\cdots\text{HOC(O)}}$ = 2.01 Å) in *trans* and the amino ($r_{\text{Cl}\cdots\text{HN}}$ = 2.44 Å) group, without any contact with the aromatic side chain. Similar hydrogen bonding motifs are shared by the *anti* terminal rotamer **TCl_ter2** (where the *anti* notation refers to the relationship between the aryl and amino groups along the C2-C3 bond), characterized by a $\angle$O1C1C2N dihedral angle equal to 74.4° and relative stability of 12.9 kJ mol^{-1} with respect to **TCl_pla1**.

Several other low-lying species have been identified (Table S2 and Fig. S6), including the left phenol conformer (**TCl_phe3**), which lies 12.4 kJ mol^{-1} higher in free energy than the lowest energy phenol structure **TCl_phe1**, although bearing a *cis* geometry of the carboxylic OH group, the commonly preferred configuration in several amino acids.[56] The most representative of them are briefly described in the Supporting Information.

The lowest energy SB structure (**TCl_zw1**), bearing an ammonium and a carboxylate group, lies 14.1 kJ mol^{-1} above **TCl_pla1**. In **TCl_zw1** the flexible chain takes on a favorable *gauche* conformation and the ammonium hydrogens establish comparatively short and strong contacts with both chloride ($r_{\text{Cl}\cdots+\text{HN}}$ = 1.94 Å) and carboxylate ($r_{\text{OCO}\cdots+\text{HN}}$ = 1.93 Å). A long-range NH$^{+}\cdots\pi$ interaction with the aromatic ring may be noted, characterized by a distance between the NH^{+} proton donor and the center of the aryl ring equal to 3.12 Å.

Recently, a related, strongly stabilizing NH$_3^{+}\cdots\pi$ interaction has been found to operate in protonated 2-phenylethylamine and related neurotransmitters, including dopamine.[12, 57-59] Moreover, in analogy with the chloride-phenylalanine complex, where the anion was found to favor the formation of the zwitterion by ca. ~80 kJ mol^{-1}, a similar stabilization of the SB form of tyrosine is likewise expected here for the [Tyr+Cl]$^{-}$ adduct, due to the close similarity of the examined chloride complexes.[18, 60]

Interestingly, deprotonation at the phenol site is much more energy demanding as evident in the SB structure **TCl_O1**, which places the chloride anion in a terminal configuration, between the ammonium group ($r_{\text{Cl}\cdots\text{HN}}$ = 1.93 Å) and the carboxylic acid ($r_{\text{Cl}\cdots\text{HOC(O)}}$ = 2.01 Å). This isomer lies 85.0 kJ mol^{-1} above **TCl_pla1**, thus discarding a significant contribution of this species to the sampled ion population.

From a comparative inspection of Fig. 2, the steady decrease of relative free energy in the couple **TCl_phe1**/**TCl_pla1**, being 7.3, 2.3, and -1.3 kJ mol^{-1} at B3LYP, B3LYP-D3 and MP2(full), respectively, may be ascribed to the comparatively improved accuracy in the treatment of non-covalent interactions, particularly crucial in the bidentate binding motif of the **TCl_pla1** structure, which presents a long-range C-H$\cdots$Cl^{-} interaction. Anyway, the close energy spacing predicted at any level underlines the presence of multiple species in the averaged ion population at 298 K.

For [Tyr+Br]⁻ and [Tyr+I]⁻, a survey of conformational landscape has been independently carried out, in order to obtain a reliable pattern of low energy species. Indeed, theory predicts the same binding motifs as described in [Tyr+Cl]⁻, though a reverse energy ordering for the lowest lying structures **TCl_pla1** and **TCl_phe1**, along with somewhat broader energy gaps with increasing anion size (Table S2-3 and Fig. S7 and S8). Accordingly, the lowest energy structures of [Tyr+Br]⁻ and [Tyr+I]⁻ adducts correspond to a phenol-bound isomer (**TBr_phe1** and **TI_phe1**). At the different levels of theory (namely B3LYP, B3LYP-D3 and MP2(full)), the free energy bias for phenol (**TBr_phe1**) as compared to plane (**TBr_pla1**) isomers is reduced from 9.1 to 4.7 and 2.1 kJ mol⁻¹ for [Tyr+Br]⁻, and from 14.3 to 5.8 and 6.8 kJ mol⁻¹, for [Tyr+I]⁻, respectively. This finding confirms the trend already observed for the [Tyr+Cl]⁻ complex.

All **TCl_phe1**, **TBr_phe1**, and **TI_phe1** present strictly similar values of dihedral angles irrespective of the halide, while the anion–phenol (X⁻···HOC$_{aryl}$) bond distances increase by 0.195 Å (X = Br) and 0.513 Å (X = I) as compared to [Tyr+Cl]⁻.

Also in the bidentate plane arrangement (**TBr_pla1** and **TI_pla1**), both the anion-ring hydrogen (X⁻···HC) and the anion-carboxyl (X⁻···HOC) distances increase by 0.217 and 0.196 Å (X = Br), and by 0.470 and 0.528 Å (X = I), respectively, as compared to [Tyr+Cl]⁻. These species are only 2.1 kJ mol⁻¹ (X = Br) and 6.8 kJ mol⁻¹ (X = I) higher in energy relative to their respective global minima (**TBr_phe1** and **TI_phe1**), 5.6 and 5.3 kJ mol⁻¹ more favourable than their respective terminal isomers (**TBr_ter1** and **TI_ter1**), and 13.2 and 11.6 kJ mol⁻¹ lower in energy than the lowest energy SB isomers (**TBr_zw1** and **TI_zw1**).

In spite of a careful search, any attempt to localize the halide anion atop the aromatic ring in [Tyr+X]⁻ failed, likely owing to repulsion with the π cloud.

[nitroTyr+X]⁻ (X= Cl, Br, I)

A similar computational analysis has been performed on [nitroTyr+X]⁻ complexes, so attaining the optimized structures depicted in Fig. 3 and Fig. S9 and S10 (X = Cl), Fig. S11 (X = Br) and Fig. S12 (X = I). Here, the presence of the nitro moiety engaged in a strong hydrogen bond with the ortho hydroxyl group changes the structural landscape, strongly stabilizing anions in plane and terminal configuration with respect to the phenol site (Table S4). Halide binding to the phenolic hydrogen hampers in fact the hydrogen bond with the nitro group.

Analogously to [Tyr+Cl]⁻, the global minimum of [nitroTyr+Cl]⁻ is the canonical, *gauche* isomer **nTCl_pla1**, which benefits from a bifurcated C$_{aryl}$H···Cl⁻···HOC(O) hydrogen bonding motif and a NH···O=C interaction, in an arrangement characterized by ∠O1C1C2N, ∠NC2C3C1' and ∠C2C3C1'C2' dihedral angles of 159.1°, -66.0° and 101.2°, respectively (Table S5). The rotation of 180° around the C$_{aryl}$-C bond weakens this arrangement by 11.3 kJ mol⁻¹ likely due to the coordination of chloride to an aromatic hydrogen made less acid by interaction with the vicinal nitro moiety (**nTCl_pla2**). The lowest energy terminal structures **nTCl_ter1** and **nTCl_ter3** (shown in Fig. 3 and S9, respectively), which feature a bidentate interaction of chloride with the carboxylic acid and the amine group, lie 6.3, and 16.8 kJ mol⁻¹ above **nTCl_pla1**, respectively. Their *anti* arrangement modifies the ∠O1C1C2N, ∠NC2C3C1' dihedral angles to -56.3°, -178.3° (**nTCl_ter1**), and -55.2°, -175.8° (in **nTCl_ter3**), respectively.

Interestingly, the position of the ring substituents relative to the side chain is almost irrelevant, as evident in the couple **nTCl_ter3** / **nTCl_ter4** (Fig. S9).

Other terminal conformers adopt a *gauche* arrangement. Among these, **nTCl_ring1** and **nTCl_ring2** (Fig. 3 and S9, respectively), represent the first examples of ring-terminal structures identified herein, where the anion is placed above the center of the ring, showing an anion-π interaction (Fig. 3). Likely, the addition of the electron-withdrawing nitro substituent to the aryl ring yields a π-acidic unit that enables chloride to interact with the π-system besides the amino and carboxylic groups (**nTCl_ring1**) or only with the amino site interacting in turn with the carboxylic

hydroxyl group (**nTCl_ring2**). However, the two structures result 7.2 and 26.0 kJ mol^{-1} respectively less favourable than **nTCl_ter1** and should thus be minor contributor to the spectra of [nitroTyr+Cl]$^{-}$ adduct. Conversely, similar binding motifs have already been found to contribute to the IRMPD spectra of halide-bound ring-fluorinated phenylalanine anions.[18]

Conversely, coordination at the phenol site, which prevents the formation of the strong intramolecular OH···ONO hydrogen bond, significantly reduces the stability, as observed for isomer **nTCl_phe1**, lying 23.1 kJ mol^{-1} above **nTCl_pla1**. This observation is in marked contrast with halide-tyrosine complexes, where binding at the phenol site is expected to contribute significantly to the ion population.

SB structures of [nitroTyr+Cl]$^{-}$ have been also identified, the lowest energy one among them (**nTCl_zw1**) is 27.7 kJ mol^{-1} higher in energy than the global minimum **nTCl_pla1**, a comparatively much larger energy difference than the 14.1 kJ mol^{-1} value found for the corresponding couple **TCl_pla1**/ **TCl_zw1** of [Tyr+Cl]$^{-}$ adduct/ in the tyrosine complex.

Deprotonation at the phenol function has been also explored and found much less favorable, with **nTCl_O1** predicted to be 81.8 kJ mol^{-1} above the global minimum **nTCl_pla1**, which does not support its contribution to any significant extent in the probed ion population.

Due to the relatively close gas-phase acidities of 2-nitrophenol, tyrosine and HCl, all within 4 kJ mol^{-1} of each other,[61] we have hypothesized a structure where the phenolic hydrogen has moved to the chloride anion so that the ensuing HCl is now involved in a hydrogen bridging interaction with both the oxygen atoms of the nitro and the phenoxide groups. However, a local minimum could not be found by geometry optimization using either the B3LYP or B3LYP-D3 functionals. Eventually, the structure ended in the transition state (**ST-1**) located along the coordinates of the proton translational reaction from an initial geometry showing a bisected hydrogen bond to the one observed in **nTCl_phe1** (Fig. S10). The imaginary frequency shows in fact displacement of H towards the phenoxide oxygen leading to a structure resembling **nTCl_phe1**.

Overall, the same trend holds for [nitroTyr+X]$^{-}$ (X= Br, I) with plane and terminal structures as the lowest energy isomers, ring configurations identified as local minima stabilized by anion-π effects, and phenol functionality as the least favorable binding site (Table S4-5; Fig. S11 and S12). Interestingly, it emerges that the more charge diffuse iodide significantly narrows the energy gaps inside the whole set of [nitroTyr+I]$^{-}$ species, with the lowest energy zwitterion isomer (**nTI_zw1**) only 2.4 kJ mol^{-1} above the phenol structure (**nTI_phe1**).

Spectral assignment

[Tyr+X]$^{-}$ (X = Cl, Br, I)

In order to ascertain the structural features of the sampled ion population, experimental IRMPD spectra, which mainly reflect the absorption of the first resonant IR photon, have been recorded and compared with the theoretical IR spectra for the lowest energy representative geometries of [Tyr+Cl]$^{-}$. The comparison covers both the IR fingerprint (Fig. 4) and OH/NH stretching (Fig. S13) ranges. A comprehensive presentation of the IR spectra of the other identified [Tyr+Cl]$^{-}$ structures (Fig. S6) is provided in Fig. S14.

For a more quantitative evaluation, the positions and intensities of the major IRMPD features are presented in Table S6, along with the computed IR transitions for the lowest energy structures, **TCl_pla1**, **TCl_phe1**, **TCl_ter1**, and **TCl_ter2**, and a brief mode description.

From the comparative inspection of Fig. 4, it emerges clearly that [Tyr+Cl]$^{-}$ does not conform to a single structure, but rather exists as a mixture of at least two low-lying canonical structures. All the main IRMPD absorptions in the mid-IR region find a counterpart in the features of the lowest

Physical Chemistry Chemical Physics Accepted Manuscript

energy plane and phenol isomers (Table S6), in agreement with their relative Gibbs energies (Table S2). The prominent, structured absorption observed at 1720 cm^{-1}, may be assigned to the υ(C=O) stretching mode of **TCl_pla1**, calculated at 1713 cm^{-1}, but also compatible with the analogous absorptions of the terminal structures **TCl_ter1** and **TCl_ter2** predicted at 1714 and 1706 cm^{-1}, respectively. The carbonyl stretching mode of either plane or terminal species is significantly redshifted when compared to protonated or potassiated tyrosine, presenting a feature at 1757 and 1744 cm^{-1}, respectively.[28, 45] Conversely, the shoulder at 1790 cm^{-1} agrees with only the υ(CO) predicted at 1781 cm^{-1} for **TCl_phe1**, a structure bearing an almost unperturbed C=O group. In addition, the IR spectra of SB structures present strong discrepancy, being characterized by the intense antisymmetric carboxylate stretch of **TCl_zw1**, expected at 1669 cm^{-1}, signature of deprotonation at the carboxylic moiety, and the υ(CO) of **TCl_O1**, blue-shifted at 1754 cm^{-1}, both inconsistent with experimental evidence. Although the zwitterionic **TCl_O1** structure is high in energy, it is interesting to note that its participation to the sampled ion population can be ruled out, based on the IRMPD spectra. In fact, ESI may deliver in the gas phase so-called kinetically trapped species, endowed with significant stability in solution, like zwitterionic structures.

The band observed at 1178 cm^{-1} arises from the phenolic OH bend, expected for **TCl_pla1** at 1166 cm^{-1}, and for **TCl_ter2** at 1171 cm^{-1}, besides the carboxylic COH bending mode coupled with NH$_2$ wagging, contributed by the **TCl_pla1** and **TCl_phe1** modes predicted at 1194 and at 1178 cm^{-1}, respectively, and compatible with the **TCl_ter2** band at 1197 cm^{-1}. The IRMPD absorption at 1250 cm^{-1} is consistent with the phenolic OH bend of **TCl_phe1**, and **TCl_ter2**, calculated at 1250 and 1223 cm^{-1}, respectively, and ring deformation of **TCl_pla1** and **TCl_ter2**, expected at 1230-1233 cm^{-1}. The envelope of intense bands between 1300 and 1400 cm^{-1} mainly comprises the ring deformation of **TCl_phe1**, predicted at 1293 cm^{-1}, the COH bending of **TCl_pla1, TCl_phe1** and **TCl_ter2**, calculated at 1352, 1397, and 1337 cm^{-1}, respectively, the COH bending mode coupled with NH$_2$ twisting of **TCl_ter2**, expected at 1365 cm^{-1}, and the CH bend of **TCl_pla1** and **TCl_ter2**, calculated at 1395 and 1379 cm^{-1}, respectively. At higher frequencies, the feature at 1503 cm^{-1} represents the CH bending of **TCl_phe1**, and **TCl_pla1**, and **TCl_ter2**, predicted at 1506-1509 cm^{-1}, while the band at 1608 cm^{-1} is mostly due to ring deformation of **TCl_phe1**, expected at 1615 cm^{-1}. Noteworthy is the absence in the IRMPD spectrum of detectable peaks for: i) the NH$_3$ umbrella mode, expected at 1438 cm^{-1} for **TCl_zw1**, and at 1594 cm^{-1} for **TCl_O1**; ii) the phenoxide C-O stretching coupled to ring CC stretching for **TCl_O1**, signature of deprotonation at the phenol functionality, predicted at 1533 and 1580 cm^{-1}; iii) the coupled CH and NH$_3$ bending modes calculated at 1121 cm^{-1} for **TCl_zw1**.[27]

In the high-energy portion of the spectrum (2800-3800 cm^{-1}), a prominent and sharp peak centered at 3663 cm^{-1} faithfully reproduces the phenol OH stretch not engaged in hydrogen bonding and theoretically predicted at 3676 cm^{-1} for the lowest energy isomer **TCl_pla1** (Fig. S13). This band may also include contributions from the terminal species **TCl_ter1** and **TCl_ter2**, calculated at 3680 and 3671 cm^{-1}, respectively. At lower frequency, the spectrum appears rather flat, with few weak and broad resonances around 3000 cm^{-1} and 3200 cm^{-1}, where the peaks for ring CH stretches (for both **TCl_pla1** and **TCl_phe1**) and carboxylic OH stretch involved in hydrogen bonding with the amino group (for **TCl_phe1**) are expected. However, the integrated area under these wide features is not negligible, and seems to confirm a substantial contribution from the plane (major) and phenol and/or terminal (minor) structures to the sampled ion population. In all cases the NH$_2$ (a)symmetric stretches hardly emerge from the background due to their low intensity (Table 1). Both the carboxylic (**TCl_pla1**) and phenolic (**TCl_phe1**) OH stretches coordinated to the anion are expected to display a marked redshift (below 2800 cm^{-1}), thus falling out of the accessible range (Table S6). Also very similar is the IR spectrum of the lowest energy SB species (**TCl_zw1**), which however should not be populated, according to theoretical predictions. Overall, although this region is not very sensitive to the structural features, and may suffer from red-shift and broadening owing

to anharmonicity and nonlinear effects. However, it provides evidence for a free phenolic OH, fully consistent with an important contribution of a plane structure to the [Tyr+Cl]⁻ spectrum.

All these results taken together indicate **TCl_pla1** and **TCl_phe1** as the most probable chloride-bound tyrosine isomers. However, the terminal isomers **TCl_ter1** and **TCl_ter2**, whose IR spectra fit large energy regions, cannot be excluded spectroscopically nor distinguished from the **TCl_pla1** isomer. However, based on relative energies, **TCl_ter1** and **TCl_ter2** should not represent a significant part of the ion population sampled at 298 K. Accordingly, the thermally averaged spectrum of [Tyr+Cl]⁻ adduct, obtained by considering contributions from all thermally accessible structures according to their relative free energy values, is also presented for comparison in Fig. S15.

The mid-IR spectra of [Tyr+Br]⁻ and [Tyr+I]⁻, which present many resemblances with [Tyr+Cl]⁻, are compared with the calculated spectra of their lowest energy representative structures in Fig. 5. The major IRMPD bands are given in Table S6 along with the calculated frequencies of the low-lying phenol (**TCl_phe1**), plane **(TCl_pla1)**, and terminal (**TCl_ter1** and **TCl_ter2)** structures, which allow the assignment of vibrational modes. As in the case of [Tyr+Cl]⁻, it turns out that an admixture of the lower energy **TCl_phe1** and **TCl_pla1** isomers dominate the IRMPD spectra of both [Tyr+Br]⁻ and [Tyr+I]⁻. However, the significantly stronger intensity of the ν(CO) at ca. 1790 cm⁻¹ that emerges with increasing halide ion size reflects the progressive depletion of **TCl_pla1** relative to **TCl_phe1** in the isomeric population (Table S2) corroborated most appropriately by the computational results at MP2 level.

In agreement with the different relative energies of the [Tyr+X]⁻ (X = Cl, Br, I) complexes, the fingerprint IRMPD spectra reflect their anion-dependent structures. Any relevant contribution of the higher energy [Tyr+X]⁻ isomers can be spectroscopically ruled out (Fig. S14).

In the NH/OH stretch spectral region (Fig. S13), the sharp feature at 3664 cm⁻¹ in the spectrum of [Tyr+Br]⁻ is associated to the free ring hydroxyl group of plane (**TBr_pla1**), but it is also compatible, as for [Tyr+Cl]⁻, with a terminal arrangement (**TBr_ter1** and **TBr_ter2**) and a SB species (**TBr_zw1**), which should be ruled out on energetic grounds. Interestingly, the higher contribution of the phenol structures in [Tyr+Br]⁻ vs [Tyr+Cl]⁻ ion populations, as deduced from relative energy and mid-infrared spectroscopic evidence, may be responsible for the larger integrated area of the broad feature detected below 3300 cm⁻¹ for [Tyr+Br]⁻.

In order to provide a deeper understanding of the solvation processes, the bonding features in complexes between neutral hydrogen donors (HR) and halide anions, [X⁻+HR], have been largely investigated in the gas phase.[62] It was thus assessed that the binding energy depends on the Brønsted acidity of HR. In particular, the binding energy was found to decrease from the smaller and more basic fluoride ion[63] to the larger and less basic chloride and iodide anions,[64-65] in parallel with the decreasing extent of covalent *vs* increasing fraction of electrostatic character of the bonding interaction. Accordingly, in the present study Cl⁻, prone to engage in a stronger hydrogen bond, shows a clear bias toward the carboxylic site of tyrosine, which is relatively more acid than the phenol group, so favouring **TCl_pla1** vs **TCl_phe1**. In contrast, the less energetic interaction of I⁻, due to the larger size, makes the coordination at the two acid functionalities of tyrosine comparably favored.[66]

Interestingly, an evident correlation between the vibrational red-shift of the CH, NH, and OH stretching mode in substituted benzenes (SB), the acidity of the aromatic molecule and the elongation of the H-bonded group has been also reported for Cl⁻-SB complexes studied by vibrational predissociation spectroscopy.[67]

An additional signature of the different strength of the halide-carboxyl contact within [Tyr+X]⁻ is the anion size-dependent red-shift of the carbonyl stretching mode. This evidence, already pointed out in other halide-bound as well as metallated amino acids,[19,68,69] has been related to the positive interaction of the carbonyl dipole moment with the ion's electric field (Stark effect), in addition to the increase in partial carboxylate character when raising the basicity from I⁻ to Br⁻ up to Cl⁻ anion.

[nitroTyr+X]⁻ (X = Cl, Br, I)

In Fig. 6, the experimental IRMPD spectrum of [nitroTyr+Cl]⁻ in the explored mid-IR range is presented along with the linear IR spectra of the low-lying canonical species, gauche plane (**nTCl_pla1**); terminal-*left* (**nTCl_ter1**); gauche, ring-terminal (**nTCl_ring1**); gauche phenol (**nTCl_phe1**); and the SB structure deprotonated at the carboxylic site (**nTCl_zw1**). A direct comparison reveals that above 1400 cm⁻¹ there is a rather good agreement between the main experimental absorptions and the computed spectra of both lowest energy isomers **nTCl_pla1** and **nTCl_ter1**, whose features are instead quite complementary in the 1000-1400 cm⁻¹ range. Vibrational assignments of low-lying **nTCl_pla1**, **nTCl_ter1** and **nTCl_ring1** are reported in Table S7.

The band appearing at 1710 cm⁻¹ is a clear signature of a carbonyl stretch predicted at 1720 cm⁻¹ for **nTCl_pla1** and at 1715 cm⁻¹ for **nTCl_ter1**, although its moderate width (Fwhm=40 cm⁻¹) suggests that **nTCl_ring1**, whose CO group is expected as low as 1698 cm⁻¹, might be also populated under our experimental conditions. The observed redshift of the carbonyl stretching mode by ca. 50 cm⁻¹ relative to protonated 3-NO₂-Tyrosine[28] is well matched by the difference observed in the spectra of [Tyr+Cl]⁻ and protonated native Tyrosine. In the range between 1400-1650 cm⁻¹, the **nTCl_pla1**, **nTCl_ter1** and **nTCl_ring1** isomers have very similar IR absorption spectra which fully fit with the experiment. According to Table S7, the strong absorbance at 1528 cm⁻¹ is due to asymmetric NO₂ stretch, the features at 1423 and 1475 cm⁻¹ are attributed to NO stretch combined with in plane bending of the ring OH group and CH bending, respectively, and the weak peak at 1610 cm⁻¹ corresponds to ring deformation.

At lower frequency, an envelope of unresolved absorbances is responsible for the strong, broad band centered at 1330 cm⁻¹, whose resolution was not improved by the use of attenuators. This complex feature includes the intense CN stretch coupled with in plane CH bending, the phenol OH bending combined with in plane CH bending, the strongly active phenol OH bending, the ring deformation, and the OH carboxylic bending, besides the NH₂ twisting. For **nTCl_pla1**, these modes are predicted at 1207, 1252, 1280, 1341, 1357, and 1392 cm⁻¹, respectively. However, the centroid of the envelope cannot be accounted for, based only on this isomer, but likely arises from **nTCl_ter1** as well, where the OH carboxylic bending redshifted at 1324 cm⁻¹ and the CH₂ wagging predicted at 1344 cm⁻¹ nicely complement the previous assignment in interpreting the experimental band. In addition, although energetically less favorable, the presence of **nTCl_ring1** cannot be discarded due to resemblance with large portion of the IRMPD spectrum.

Clear marks that coordination has not occurred at the phenol site (**nTCl_phe1**) nor that SB isomers (**nTCl_zw1**, **nTCl_zw1**, and **nTCl_O1**) can appreciably contribute to the ion population derive from the evidence that none of these structures have calculated spectra that match the experimental spectrum (Fig. 6). Comparison with other computed structures shown in Fig. S16 suggests that they do not appreciably contribute to the sampled ion population.

The IRMPD spectra of [nitroTyr+Br]⁻ and [nitroTyr+I]⁻ are presented against the IR spectra of the lowest energy species, the canonical isomers **nTBr_pla1**, **nTBr_ter1**, **nTBr_ring1**, **nTBr_ter2** and **nTI_pla1**, **nTI_ter1**, **nTI_ring1**, **nTI_ter2**, respectively (Fig. S17). In both cases, and similarly to [nitroTyr+Cl]⁻, it turns out that a mixture of **nTBr_pla1** (**nTI_pla1**) and **nTBr_ter1** (**nTI_ter1**) are likely present in the ESI sampled ion population. Interestingly, the strong absorbance due the carbonyl stretch at 1733 cm⁻¹ (X = Br) and 1743 cm⁻¹ (X = I) is structured with a weak peak on the red side at 1698 and 1705 cm⁻¹, respectively, that may be related to the contribution of **nTBr_ring1** (**nTI_ring1**), expected at relatively lower concentration. According to the IR spectra presented in Fig. S18, any appreciable contribution of other higher energy structures can be safely ruled out.

Overall, although the anion size shows little consequence on the adopted arrangement of [nitroTyr+X]$^-$ (X = Cl, Br, I), the observed blue shift of the carbonyl stretching mode with increasing anion size confirms that the strength of the contact between the carboxylic hydrogen and the halide decreases, namely with decreasing gas phase basicity of X$^-$.

Conclusions

The halide complexes of both Tyr and nitroTyr reveal a variety of bonding motifs thoroughly explored by computations at three different levels, B3LYP/6-311++G(d,p), B3LYP-D3/6-311++G(d,p), and MP2(full)//6-311++G(d,p)//B3LYP/6-311++G(d,p). The experimental tool to assay the six distinct families of clusters, [Tyr+X]$^-$ and [nitroTyr+X]$^-$ (where X = Cl, Br, I), has relied on vibrational spectroscopy of the mass selected ions obtained by ESI. The IRMPD spectra were analyzed by comparison with the calculated IR spectra for the array of plausible geometries. In the general pattern of various binding motifs the lowest energy and represented structures correspond to 'plane' and 'phenol' geometries. The first class is characterized by the halide engaged in a CH$\cdots$X$^-\cdots$HOC(O) interaction with both a ring hydrogen and a carboxyl group. In the second coordination mode the halide is simply bound to the hydroxyl function on the aromatic ring. As another possible contribution one should take into account a 'terminal' structure involving only the amino acidic end in the general NH$\cdots$X$^-\cdots$HOC(O) arrangement. It is interesting to note that the lowest energy geometries, 'plane' and 'phenol', both involve the aromatic ring that is the side chain substituent that remains exposed also when tyrosine is part of a peptide or protein. The PTM yielding nitroTyr strongly affects the properties of the ring, in the first place by competing for hydrogen bonding to the ring OH group. Overall the following major points may be evinced: (i) 'plane' and 'phenol' structures are major contributors to the [Tyr+X]$^-$ ion population; (ii) the relative weight of 'plane' and 'phenol' structures is sensitive to the nature of X, favoring the 'phenol' species with increasing size of X; (iii) the presence of the 3-nitro substituent has a dramatic effect in inhibiting X$^-$ association to the ring OH while also directing the interaction with a ring hydrogen in preferential para position with respect to the electron withdrawing group; (iv) only in the presence of the nitro group, depleting π-electron density, do anion-π interactions play a role as additional binding motif.

Hopefully, an insight is provided into the intrinsic nature of non covalent interactions involving ubiquitous halide ions and Tyr/nitroTyr. Tyrosine residues may line the cavity within biological and synthetic ion channels and the present data show that a variety of binding motifs may be at play and be tuned to achieve specific functioning.

Acknowledgements

References

1 P.A. Gale, *Acc. Chem. Res.,* 2011, **44**, 216–226

2 H. T. Chifotides and K. R. Dunbar, *Acc. Chem. Res.*, 2013, **46**, 894–906.

3 E. M. Milner, M. G. D. Nix and C. E. H. Dessent, *J. Phys. Chem. A*, 2012, **116**, 801-809.

4 J. Oomens, B.G. Sartakov, G. Meijer and G. Von Helden, *Int. J. Mass Spectrom.,* 2006, **254**, 1-19.

5 L. MacAleese and P. Maitre, *Mass Spectrom. Rev.,* 2007, **26**, 583–605.

6 N.C. Polfer, *Chem. Soc. Rev.,* 2011, **40**, 2211–2221.

7 J. Roithova, *Chem. Soc. Rev.*, 2012, **41**, 547–559.

8 B. Chiavarino, M. E. Crestoni, O. Dopfer, P. Maitre and S. Fornarini, *Angew. Chem., Int. Ed.* 2012, **51**, 4947 –4949.

9 B. Chiavarino, M. E. Crestoni, S. Fornarini, S. Taioli, I. Mancini and P. Tosi, *J. Chem. Phys.,* 2012, **137**, 024307.

10 F. Lanucara, B. Chiavarino, D. Scuderi, P. Maitre, S. Fornarini and M. E. Crestoni, *Chem. Commun.,* 2014, **50**, 3845-3848.

11 D. Corinti, C. Coletti, N Re, B. Chiavarino, M. E. Crestoni and S. Fornarini, *Chem. Eur. J.,* 2016, **22**, 3794 – 3803.

12 B. Chiavarino, M. E. Crestoni, M. Schütz, A. Bouchet, S. Piccirillo, V. Steinmetz, O. Dopfer and S. Fornarini, *J. Phys. Chem. A,* 2014, **118**, 7130−7138.

13 D. Scuderi, E. Bodo, B. Chiavarino, S. Fornarini and M. E. Crestoni, *Chem. Eur. J.,* 2016, **22**, 17239-17250.

14 B. Chiavarino, M. E. Crestoni, S. Fornarini, D. Scuderi and J.-Y. Salpin, *Inorg. Chem.*, 2015, **54**, 3513−3522.

15 M. F. Bush, J. Oomens and E. R. Williams, *J. Phys. Chem. A,* 2009, **113**, 431-438.

16 C. Kapota, J. Lemaire, P. Maitre and G. Ohanessian, *J. Am. Chem. Soc.*, 2004, **126**, 1836-1842.

17 R. C. Dunbar, A. C. Hopkinson, J. Oomens, C. K. Siu, K. W. M. Siu, J. D. Steill, U. H. Vertek and J. F. Zhao, *J. Phys. Chem. B,* 2009, **113**, 10403-10408.

18 M. Burt, K. Wilson, R. Marta, M. Hasan, W. S. Hopkins and T. McMahon, *Phys. Chem. Chem. Phys.,* 2014, **16**, 24223-24234.

19 J. T. O'Brien, J. S. Prell, G. Berden, J. Oomens and E. R. Williams, *Int. J. Mass Spectrom.*, 2010, **297**, 116-123.

20 J. Schmidt and S. R. Kass, *J. Phys. Chem A,* 2013, **117**, 4863-4869.

21 B. Chiavarino, M. E. Crestoni, P. Maitre and S. Fornarini, *Int. J. Mass Spectrom.,* 2013, **354-355**, 62-69.

22 M. E. Crestoni, B. Chiavarino, S. Fornarini, *Pure Appl. Chem*., 2015, **87**, 379-390.

23 B. Chiavarino, M.E. Crestoni, S. Fornarini, F. Lanucara, J. Lemaire, P. Maitre and D. Scuderi, *Chem. Eur. J.,* 2009, **15**, 8185–8195.

24 M. L. Stover, V. E. Jackson, M. H. Matus, M. A. Adams, C. J. Cassady and D. A. Dixon, *J. Phys. Chem. B,* 2012, **116**, 2905−2916.

25 Z. Tian and S. R. Kass, *J. Am. Chem. Soc.,* 2008, **130**, 10842–10843.

26 J. Oomens, J. D. Steill and B. Redlich, *J. Am. Chem. Soc.,* 2009, **131**, 4310-4319.

27 J. D. Steill and J. Oomens, *J. Am. Chem. Soc.,* 2009, **131**, 13570-13571.

28 R. K. Sinha, B. Chiavarino, M. Elisa Crestoni, D. Scuderi and S. Fornarini, *Int. J. Mass Spectrom.,* 2011, **308**, 209-216.

29 J. Lemaire, P. Boissel, M. Heninger, G. Mauclaire, G. Bellec, H. Mestdagh, A. Simon, S. Le Caer, J. M. Ortega, F. Glotin and P. Maitre, *Phys. Rev. Lett.,* 2002, **89**, 273002.

30 L. Mac Aleese, A. Simon, T. B. McMahon, J.-M. Ortega, D. Scuderi, J. Lemaire and P. Maitre, *Int. J. Mass Spectrom.* 2006, **249/250**, 14-20.

31 P. Maitre, J. Lemaire and D. Scuderi, *Physica Scripta,* 2008, **78**, 058111/1-058111/6.

32 R. K. Sinha, P. Maitre, S. Piccirillo, B. Chiavarino, M. E. Crestoni and S. Fornarini, *Phys. Chem. Chem. Phys.,* 2010, **12**, 9794-9800.

33 J. S. Prell, J. T. O'Brien and E. R. Williams, *J. Am. Soc. Mass Spectrom.,* **2010**, **21**, 800-809.

34 D. A. Case, T. Darden, T. E. Cheatham, C. Simmerling, J. Wang, R. E. Duke, R. Luo, K. M. Merz, B. Wang, D. A.Pearlman, et al. *Amber 8 User's Manual*; University of California: San Francisco, CA, 2004.

35 J. Wang, R. M. Wolf, J. W. Caldwell, P. A. Kollman and D. A. Case, *J. Comput. Chem.,* 2004, **25**, 1157−1174.

36 F. Neese, *"ORCA," an ab initio, Density Functional and Semiempirical Program Package* (v. 2.6-35) Universitat Bonn: Bonn, Germany, 2007.

37 F. Neese, *WIREs Comput. Mol. Sci.,* 2012, **2**, 73−78.

38 F. Weigend and R. Ahlrichs, *Phys. Chem. Chem. Phys.*, 2005, **7** , 3297–3305.

39 O. Dopfer, N. Solca, J. Lemaire, P. Maitre, M. E. Crestoni and S. Fornarini, *J. Phys. Chem. A,* 2005, **109**, 7881−7887.

40 B. Gregori, L. Guidoni, B. Chiavarino, D. Scuderi, E. Nicol, G. Frison, S. Fornarini and M. E. Crestoni, *J. Phys. Chem. B,* 2014, **118**, 12371-12382.

41 C. Blondel, P. Cacciani, C. Delsart and R.Trainham, *Phys. Rev. A*, 1989, **40**, 3698.

42 R. J. Pelez, C. Blondel, C. Delsart and C. Drag, *J. Phys. B: Atom. Mol. Opt. Phys*., 2009, **42**, 125001.

43 J.D.D. Martin and J.W. Hepburn, *J. Chem. Phys.,* 1998, **109**, 8139-8142.

44 N. C. Polfer, B. Paizs, L. C. Snoek, I. Compagnon, S. Suhai, G. Meijer, G. von Helden and J. Oomens, *J. Am. Chem. Soc.,* 2005, **127**, 8571 −8579.

45 R. C.Dunbar, *J. Phys. Chem. A,* 2000, **104**, 8067 −8074.

46 P. B. Armentrout, Bo Yang and M. T. Rodgers, *J. Phys. Chem. B,* 2013, **117**, 3771−3781.

47 J. D. Chai and M. Head-Gordon, *Phys. Chem. Chem. Phys.,* 2008, **10**, 6615-6620.

48 M. Head-Gordon, J. A. Pople and M. J. Frisch, *Chem. Phys. Lett.,* 1988, **153**, 503-506.

49 M. Walker, A. Sen, A. J. A. Harvey and C. E. H. Dessent, *Chem. Phys. Lett.,* 2013, **588**, 43-46.

50 C. Ruan and M. T. Rodgers, *J. Am. Chem. Soc.,* 2004, **126**, 14600-14610.

51 G. Bouchoux, *Mass Spectrom. Rev.,* 2012, **31**, 391–435.

52 C. Perez, S. Mata, C. Cabezas, J. C. Lopez and J. L. Alonso, *J. Phys. Chem. A,* 2015, **119**, 3731-3735.

53 Y. Inokuchi, Y. Kobayashi, T. Ito and T. Ebata, *J. Phys. Chem. A,* 2007, **111**, 3209-3215.

54 A Abo-Riziq, L. Grace, B. Crews†, M. P. Callahan, T. Mourik and M. S. de Vries, *J. Phys. Chem. A,* 2011, **115**, 6077–6087.

55 Y. Shimozono, K. Yamada, S.-i. Ishiuchi, K. Tsukiyama and M. Fujii, *Phys. Chem. Chem. Phys.,* 2013, **15**, 5163-5175.

56 F. Gabas, R. Conte and M. Ceotto, *J. Chem. Theory Comput.* 2017, **13**, 2378-2388.

57 A. Bouchet, M. Schutz, B. Chiavarino, M. E. Crestoni, S. Fornarini and O. Dopfer, *Phys. Chem. Chem. Phys.*, 2015, **17**, 25742-25754.

58 M. Schütz, A. Bouchet, B. Chiavarino, M. E. Crestoni, S. Fornarini and O. Dopfer, *Chem. Eur. J.,* 2016, **22**, 8124-8136.

59 A. Lagutschenkov, J. Langer, G. Berden, J. Oomens and O. Dopfer, *Phys. Chem. Chem. Phys.,* 2011, **13**, 2815-2823.

60 L. C. Snoek, E. G. Robertson, R. T. Kroemer and J. P. Simons, *Chem Phys Lett.,* 2000, **321**, 49-56.

61 NIST Chemistry WebBook, NIST Standard Reference Database, Number 69 (Eds.: P. J. Linstrom, W. G. Mallard) National Institute of Standards and Technology, Gaithersburg MD, 20899, http://webbook.nist.gov.

62 S. Tshepelevitsh, A. Trummal, K. Haav, K. Martin and I. Leito, *J. Phys. Chem. A,* 2017, **121**, 357−369.

63 J. W. Larson and T. B. McMahon, *J. Am. Chem. Soc.,* 1983, **105**, 2944-2950.

64 J. W. Larson and T. B. McMahon, *J. Am. Chem. Soc.,* 1984, **106**, 517-521.

65 G. Caldwell and P. Kebarle *J. Am. Chem. Soc*., 1984, **106**, 961-969.

66 J. W. Larson and T. B. McMahon, *J. Am. Chem. Soc.,* 1987, **109**, 6230-6236.

67 C. Emmeluth, B. L. J. Poad, C. D. Thompson and E. J. Bieske, *J. Phys. Chem. A*, 2007, **111**, 7322-7328.

68 M. F. Bush, J. Oomens, R. J. Saykally and E. R. Williams, *J. Phys. Chem. A,* 2008, **112**, 8578-8584.

69 M. T. Rodgers, P. B. Armentrout, J. Oomens and J. D. Steill, *J. Phys. Chem. A,* 2008, **112**, 2258-2267.
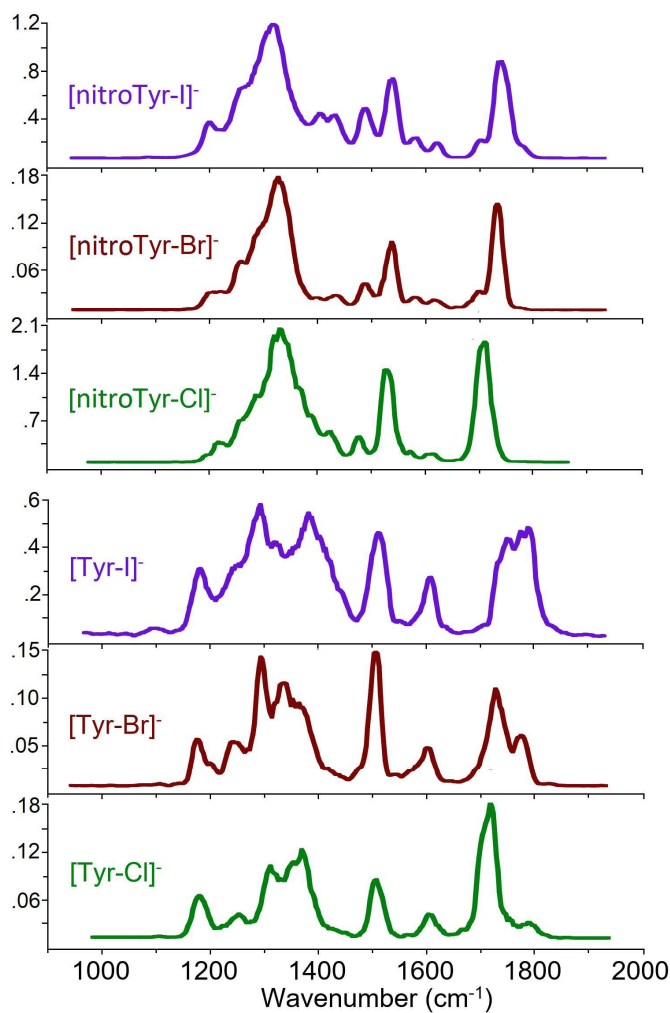
Fig. 1 Experimental IRMPD spectra of [Tyr+X]⁻ and [nitroTyr+X]⁻ (X= Cl, Br, I) complexes in the 950-1950 cm⁻¹ range.

Physical Chemistry Chemical Physics Accepted Manuscript

Fig. 2 Optimized geometries for selected isomers of [Tyr+Cl]⁻. Relative enthalpies and relative free energies (bracketed) at the B3LYP/6-311++G(d,p) (in red), B3LYP-D3/6-311++G(d,p) (in blue) and MP2//B3LYP/6-311++G(d,p) (in black) levels are provided at 298 K in kJ mol^{-1}. Interatomic bond distances, marked by dashed lines, are reported in Å.
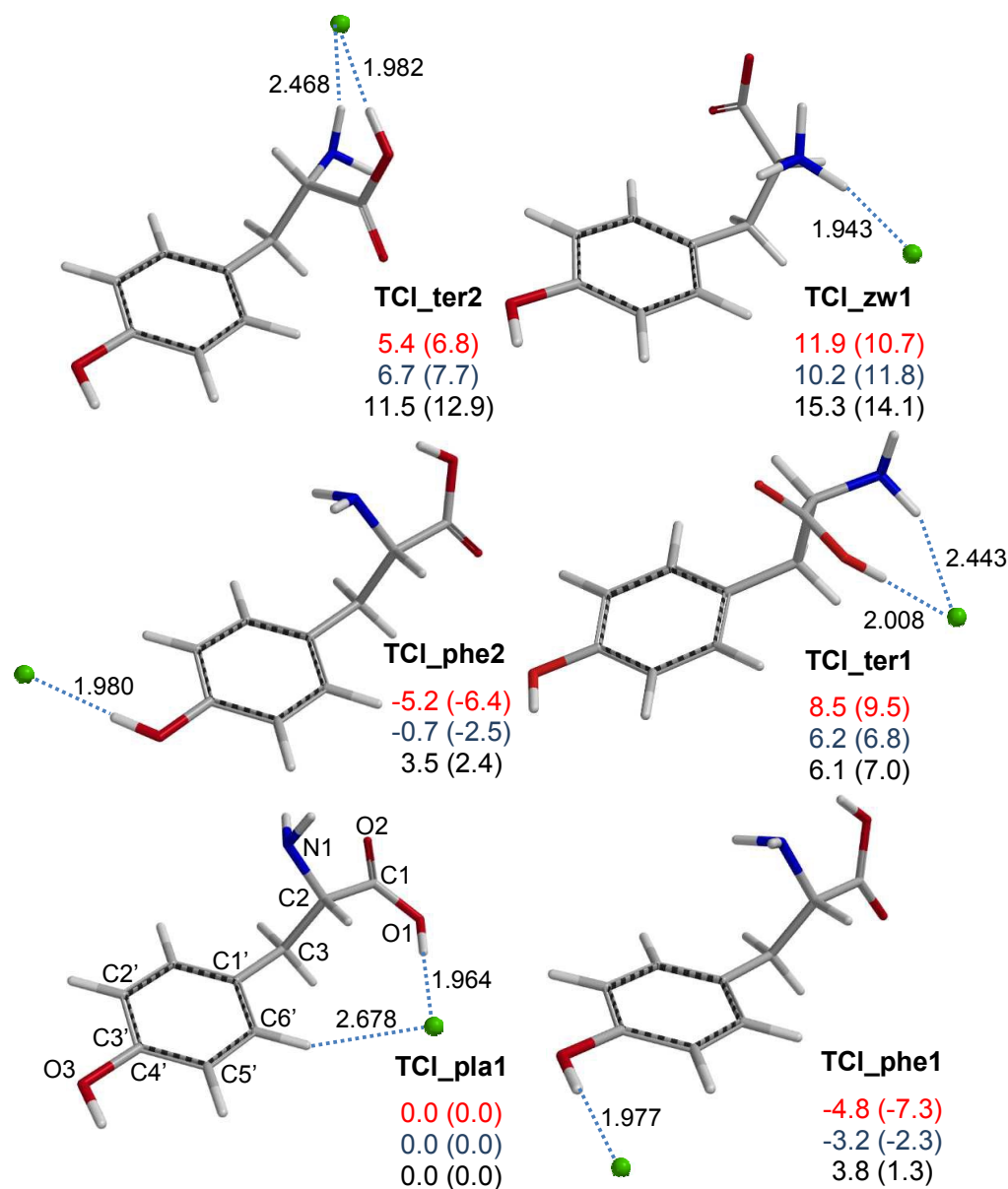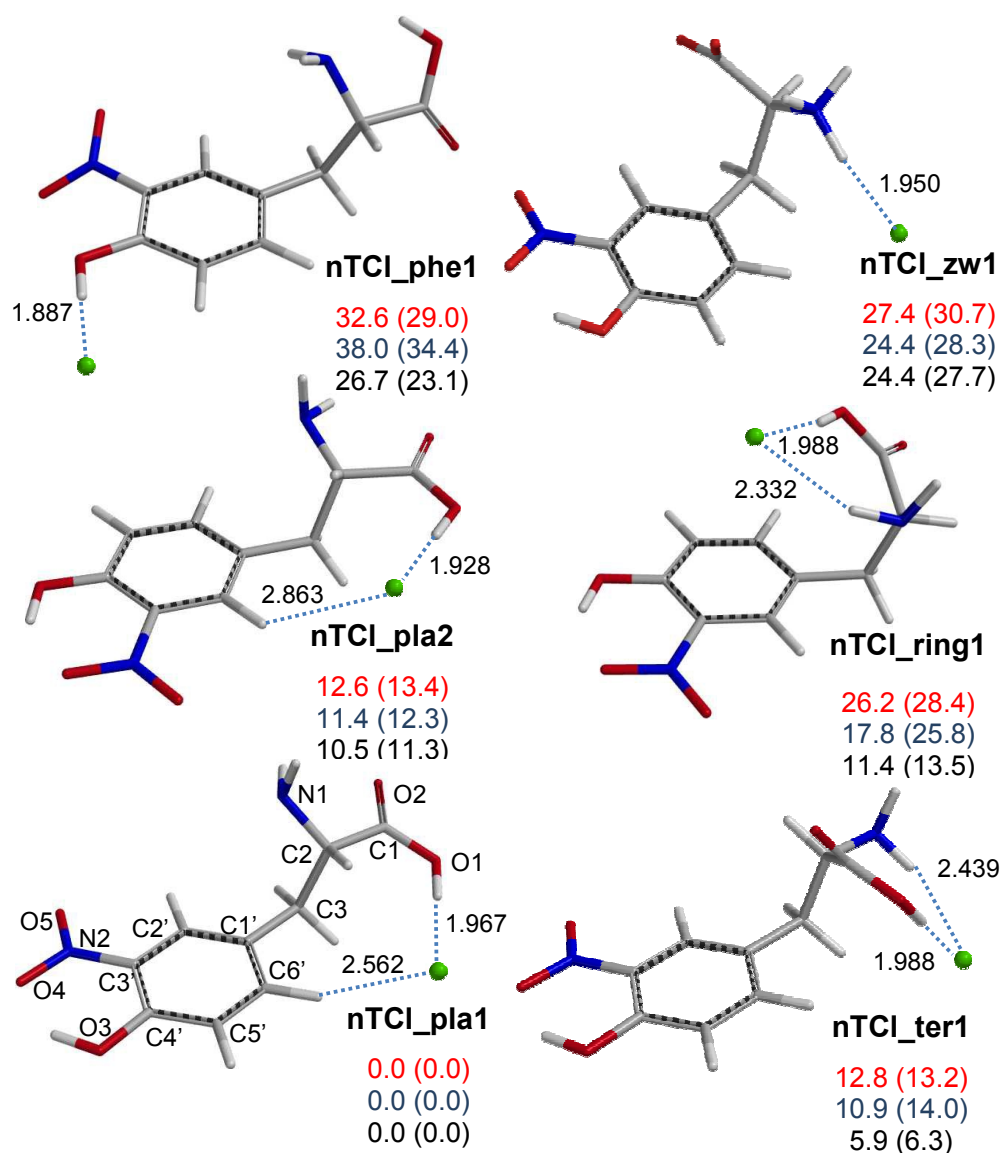
Fig. 3 Optimized geometries for selected isomers of [nitroTyr+Cl]⁻. Relative enthalpies and relative free energies (bracketed) at the B3LYP/6-311++G(d,p) (in red), B3LYP-D3/6-311++G(d,p) (in blue) and MP2//B3LYP/6-311++G(d,p) (in black) levels are provided at 298 K in kJ mol^{-1}. Interatomic bond distances, marked by dashed lines, are reported in Å.

Fig. 4 Experimental IRMPD spectrum (green profile) of chloride-bound tyrosine adduct, [Tyr+Cl]⁻, compared with IR spectra [km mol⁻¹] for **TCl_pla1**, **TCl_phe1**, **TCl_ter1**, **TCl_ter2**, **TCl_zw1** and **TCl_O1** structures obtained at the B3LYP/6-311++G(d,p) level of theory and scaled by a factor of 0.978. The scale of the y-axis is the same for all theoretical IR spectra. The pale green profile reports the experimental [Tyr+Cl]⁻ spectrum. Relative enthalpies and relative free energies (bracketed) at the B3LYP/6-311++G(d,p) (in red), B3LYP-D3/6-311++G(d,p) (in blue) and MP2//B3LYP/6-311++G(d,p) (in black) levels are provided at 298 K in kJ mol⁻¹.

A)

TBr_zw1

15.1 (18.2)
8.2 (10.8)
15.0 (15.3)

TBr_ter2

12.1 (14.9)
8.2 (10.8)
10.2 (12.9)

TBr_ter1

14.9 (17.1)
8.5 (12.1)
5.4 (7.7)

TBr_pla1

7.8 (9.1)
2.6 (4.7)
0.8 (2.1)

TBr_phe1

0.0 (0.0)
0.0 (0.0)
0.0 (0.0)

B)

TI_zw1

20.3 (24.1)
13.2 (16.6)
14.6 (18.4)

TI_ter2

18.5 (21.0)
10.3 (11.1)
9.7 (12.1)

TI_ter1

15.3 (17.9)
9.7 (11.3)
9.4 (12.1)

TI_pla1

11.9 (14.3)
5.1 (5.8)
4.5 (6.8)

TI_phe1

0.0 (0.0)
0.0 (0.0)
0.0 (0.0)

1000   1200   1400   1600   1800   2000   1000   1200   1400   1600   1800   2000
/ cm^{-1} / cm^{-1}

Fig. 5 Experimental IRMPD spectrum of: [Tyr+Br]$^-$ (brown profile, panel A) compared with IR spectra [km mol^{-1}] for **TBr_phe1**, **TBr_pla1**, **TBr_ter1**, **TBr_ter2**, and **TBr_zw1** structures; [Tyr+I]$^-$ (purple profile, panel B) compared with IR spectra [km mol^{-1}] for **TI_phe1**, **TI_pla1**, **TI_ter1**, **TI_ter2**, and **TI_zw1** structures. Theoretical vibrational modes were obtained at the B3LYP/6-311++G(d,p) level of theory and scaled by a factor of 0.978. The scale of the y-axis is the same for all theoretical IR spectra. Relative enthalpies and relative free energies (bracketed) at the B3LYP/6-311++G(d,p) (in red), B3LYP-D3/6-311++G(d,p) (in blue) and MP2//B3LYP/6-311++G(d,p) (in black) levels are provided at 298 K in kJ mol^{-1}.
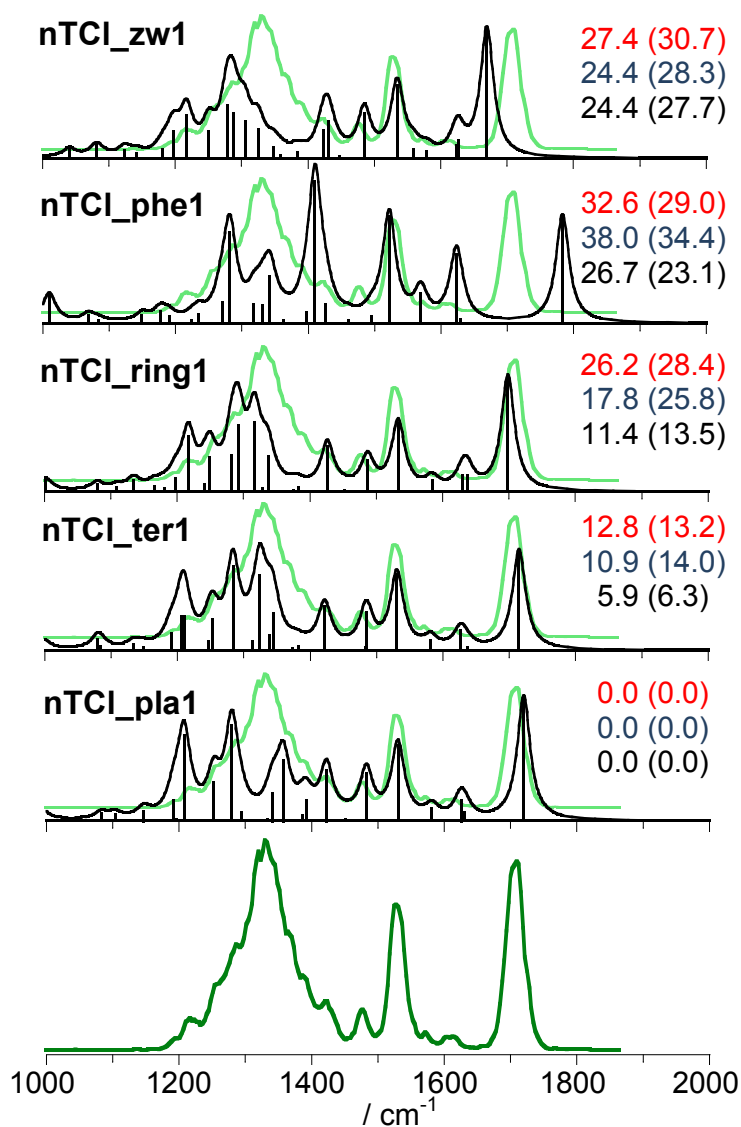
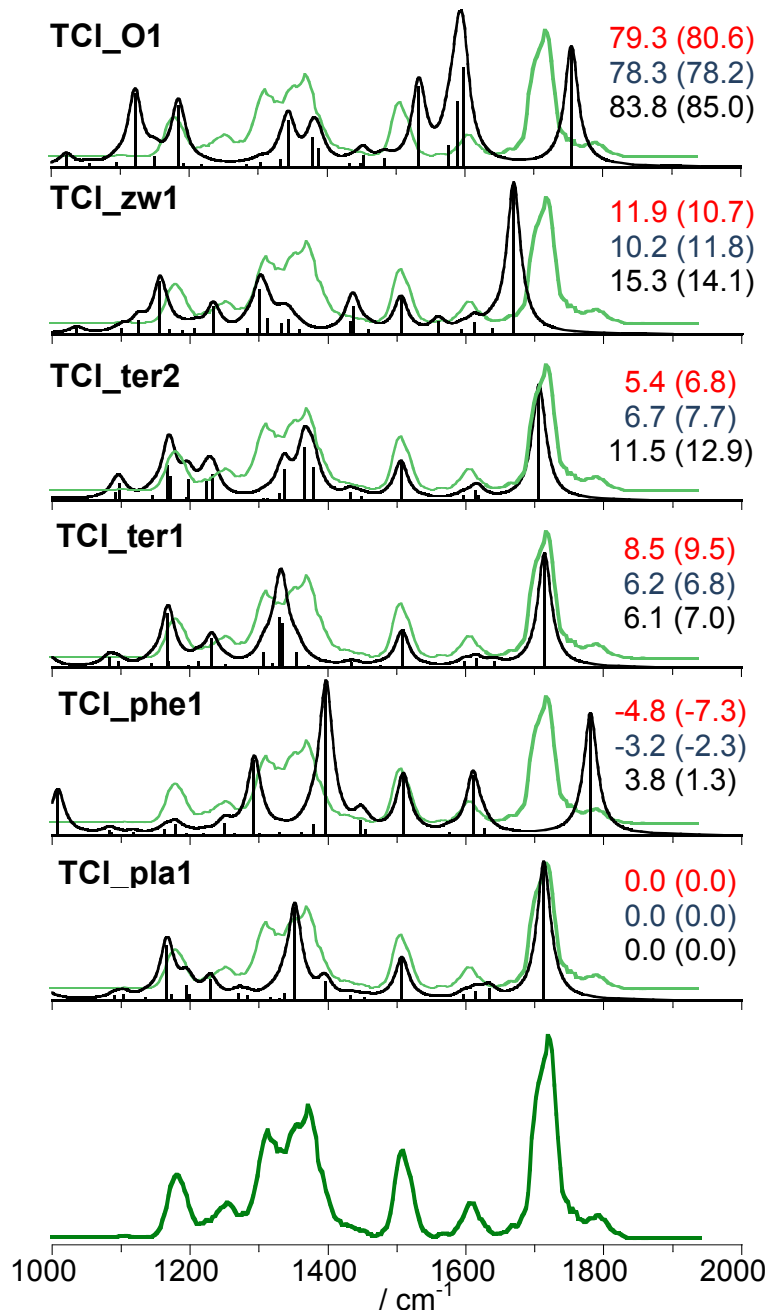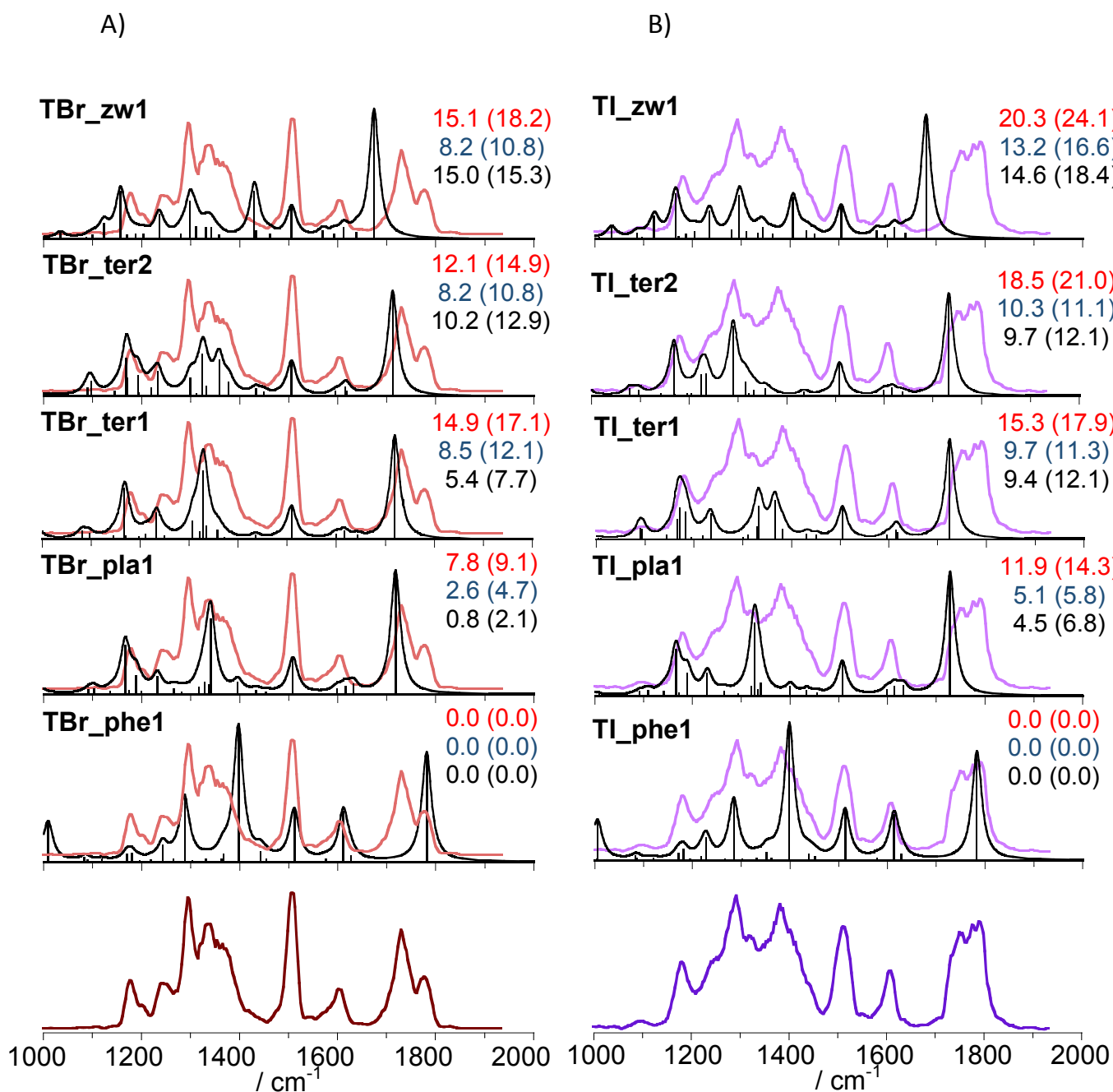**Fig. 6** Experimental IRMPD spectrum (green profile) of chloride-bound 3-NO$_2$-tyrosine adduct, [nitroTyr+Cl]$^-$, compared with IR spectra [km mol^{-1}] for **nTCl_pla1**, **nTCl_ter1**, **nTCl_ring1**, **nTCl_phe1** and **nTCl_zw1** structures obtained at the B3LYP/6-311++G(d,p) level of theory and scaled by a factor of 0.978. The scale of the y-axis is the same for all theoretical IR spectra. The pale green profile reports the experimental [nitroTyr+Cl]$^-$ spectrum. Relative enthalpies and relative free energies (bracketed) at the B3LYP/6-311++G(d,p) (in red), B3LYP-D3/6-311++G(d,p) (in blue) and MP2//B3LYP/6-311++G(d,p) (in black) levels are provided at 298 K in kJ mol^{-1}.

Table 1 Experimental IRMPD resonances and calculated (at B3LYP/6-311++G(d,p) level of theory) vibrational frequencies for the low-lying isomers **TCl_pla1**, **TCl_phe1**, **TCl_ter1** and **TCl_ter2** of [Tyr+Cl]$^-$ adduct.

	[Tyr+Cl]$^-$				
IRMPD[a]	Calculated[a,b]				Vibrational mode
	TCl_pla1	**TCl_phe1**	**TCl_ter1**	**TCl_ter2**	
1105 (low)	1104 (20)		1083 (32)	1097 (53)	NH$_2$ wagging
1178				1168 (112)	CH in plane bend
	1166 (176)		1168 (172)	1171 (77)	OH phenol bend
	1194 (47)	1178 (33)		1197 (66)	OH carboxyl bend + NH$_2$ wagging
1250		1250 (37)		1223 (57)	OH phenol bend
	1230 (64)		1232 (90)	1233 (80)	ring def
	1270 (21)				NH$_2$ twist
1312		1293 (238)	1307 (45)		ring def
1358	1336 (22)				CH in plane bend
	1352 (293)		1329 (159)	1337 (96)	OH carboxyl bend
			1334 (138)		OH carboxyl bend+OH phenol bend
				1365 (168)	COO-H bend + NH$_2$ twisting
1376		1378 (32)			OH phenol bend
	1395 (60)		1355 (46)	1379 (102)	CH bend
		1397 (474)			OH carboxyl bend
1451 (shoulder)		1447 (46)			OH phenol bend
1507	1507 (132)	1509 (185)	1507 (113)	1506 (120)	CH in plane bend
1608	1615 (26)	1610 (190)	1626 (26)	1615 (29)	ring def
	1633 (35)	1627 (22)			NH$_2$ scissor
1720	1713 (442)		1714 (364)	1706 (368)	C=O stretch
1790		1781 (389)			C=O stretch
	2710 (1871)		2850 (1705)	2759 (1879)	OH carboxyl stretch
		2751 (2962)			OH phenol stretch
			2918 (38)		CH stretch
	2898 (32)	2884 (29)			CH$_2$ symm stretch
	2994 (44)	2998 (21)		2994 (32)	CH asymm stretch
3008	3004 (42)		3005 (29)		CH symm stretch
3060	3046 (21)	3037 (32)			CH symm stretch
3200 (broad)		3242 (343)			OH carboxyl stretch
3272			3239 (218)	3242 (209)	NH$_2$ symm stretch
3330			3381 (20)	3368 (25)	NH$_2$ asymm stretch
3663	3676 (45)		3680 (48)	3671 (47)	OH phenol stretch

[a] In cm^{-1}. [b] The reported intensities given in parentheses are in km mol^{-1}. Bands with an intensity lower than 20 km mol^{-1} are not included. Frequencies are scaled by a factor of 0.978.

Physical Chemistry Chemical Physics Accepted Manuscript

TOC
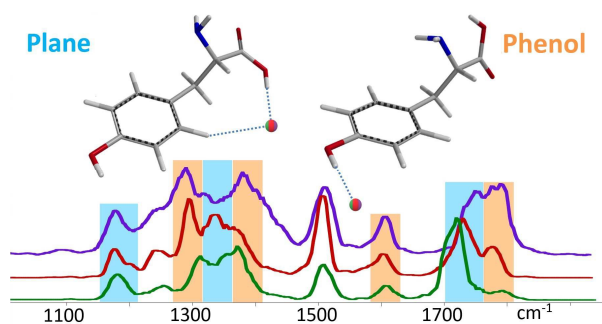
IRMPD spectra and calculations reveal the binding motifs of halide ions to tyrosine and its nitro derivative, 3-nitro-tyrosine.

23